Laser and Particle Beams (2009), *27*, 379–391. Printed in the USA.

doi:10.1017/S0263034609000494

Intense heavy ion beams as a pumping source for short wavelength lasers

A. ADONIN,[1,3] V. TURTIKOV,[2] A. ULRICH,[4] J. JACOBY,[1] D.H.H. HOFFMANN,[3,5] AND J. WIESER[6]

[1]Johann Wolfgang Goethe-Universität, Frankfurt am Main, Germany
[2]Institute for Theoretical and Experimental Physics (ITEP), Moscow, Russia
[3]Gesellschaft für Schwerionenforschung (GSI), Darmstadt, Germany
[4]Physik Department E12, Technische Universität München (TUM), Garching, Germany
[5]Technische Universität Darmstadt (TUD), Germany
[6]Coherent GmbH, München, Germany

(RECEIVED 5 January 2009; ACCEPTED 25 March 2009)

Abstract

The high energy loss of heavy ions in matter as well as the small angular scattering makes heavy ion beams an excellent tool to produce almost cylindrical and homogeneously excited volumes in matter. This aspect can be used to pump short wavelength lasers. For the first time, a beam of heavy ions was used to pump a short wavelength gas laser in an experiment performed at the GSI ion accelerator facility in December 2005. In this experiment, the well-known KrF* excimer laser was pumped with an intense uranium beam. Pulses of an uranium beam compressed down to 110 ns (full width at half maximum) with initial particle energy of 250 MeV per nucleon were stopped inside a gas laser cell. A mixture of an excimer laser premix gas (95.5%Kr + 0.5%F_2) and a buffer gas (Ar) in different proportions was used as the laser gas. The maximum beam intensity reached in the experiment was 2.5×10^9 particles per pulse, which resulted in 34 J/g specific energy deposited in the laser gas. The laser effect on the transition at $\lambda = 248$ nm has been successfully demonstrated by various independent methods. There, the laser threshold was reached with a beam intensity of 1.2×10^9 particles per pulse, and the energy of the laser pulse of about 2 mJ was measured for an ion beam intensity of 2×10^9 particles per pulse. As a next step, it is planned to reduce the laser wavelength down to the vacuum ultraviolet spectral region, and to proceed to the excimer lasers of the pure rare gases. The perspectives for such experiments are discussed and the detailed estimations for Xe and Kr cases are given. We believe that the use of heavy ion beams as a pumping source may lead to new pumping schemes on the higher lying level transitions and considerably shorter wavelengths, which rely on the high cross sections for multiple ionization of the target species.

Keywords: Excimer laser; Heavy ion beam; Laser threshold; Pumping power; Spontaneous and stimulated emission.

1. INTRODUCTION

Lasers cover a wide spectral range from the infrared to X-rays. Various types of pumping sources from regular electrical discharges (Rocca *et al.*, 1994; Wagner *et al.*, 1996), high power lasers to the flux of nuclear fusion fragments, provided by pulsed reactor facilities (Young, 1981; Karelin *et al.*, 1997) have been studied, depending on the power density required for the laser scheme or the planned application of the laser. In general, the shorter the wavelength of the laser the higher the power density required for pumping. As an alternative to laser induced plasmas that are meanwhile routinely used for pumping short wavelength lasers (Kuehl *et al.*, 2007; Neumayer *et al.*, 2005), heavy ion beams may be considered as a pumping source, which can also provide high power densities in a target material (Tahir *et al.*, 2007). In this work, the first successful operation of a KrF* excimer laser at $\lambda = 248$ nm pumped with an intense, high energy uranium ion beam (Ulrich *et al.*, 2006*a*, 2006*b*; Adonin *et al.*, 2007*a*) is described in detail.

The KrF* excimer laser is known for more than 30 years and well studied with electron beam and gas discharge pumping (Brau, 1984). The capability of KrF* laser systems to reach a high level (more than 100 kJ) of the output energy was studied with the electron beam pumping (Sullivan, 1987). These systems were in the particular interest of the laser-fusion laboratories. Due to the short wavelength, relatively high conversion efficiency, and high output power

Address correspondence and reprint requests to: A. Adonin, Gesellschaft für Schwerionenforschung, Planckstrasse 1, D-64291 Darmstadt, Germany. E-mail: a.adonin@gsi.de

KrF* laser systems were considered as a fast ignition driver for inertial confinement fusion (ICF) (Sullivan *et al.*, 1993).

Following the fast ignition ICF concept with KrF* laser, a number of experiments were recently performed in the GARPUN-MTW laser facility (Zvorykin *et al.*, 2007). Also, the high-energy KrF* laser there was used for producing shock waves in liquids and for studying hydrodynamic instabilities such as Rayleigh-Taylor and Richtmyer-Meshkov (Zvorykin *et al.*, 2008). The development of these instabilities on the target surface is one of the key-problem for ICF.

A series of laser experiments is planned at Gesellschaft für Schwerionenforschung (GSI, Darmstadt, Germany) ion accelerator facility in the context of plasma physics studies. These studies aim at the production and investigation of high energy densities in matter in general (Hoffmann *et al.*, 2005). Several aspects of the formation of plasmas, induced by heavy ion beams, have been extensively studied (Ulrich *et al.*, 1987; Jacoby *et al.*, 1990, 1995; Tahir *et al.*, 2005, 2007). Short wavelength lasers pumped with ion beams may also be used as a sensitive tool for studying ion beam induced plasmas, because population inversion and laser effect only occur under specific conditions with respect to plasma density and temperature, electron density and temperature, as well as opacity of the target material at the laser wavelength. A comparison of measured laser parameters with model calculations can therefore provide insight into the excitation and relaxation processes in ion beam induced plasmas (Ulrich *et al.*, 2006*a*).

The basic idea of heavy ion beam pumping of gas lasers is to use the specific features of ion interaction with matter. First, heavy ions have a very high energy loss in matter, which scales quadratically with the charge of the projectile that allows achieving high pumping power densities in the laser medium. Second, heavy ions have the ability to produce non-thermal excitation of atoms and molecules in the target medium. And finally, heavy projectiles propagate with small angular scattering in the medium, which in combination with ion beam focusing and the dependence of energy deposition from the projectiles energy results in an almost cylindrical and homogeneously excited volume along the ion beam axis (Tahir *et al.*, 2005). This volume can be well matched with the mode volume of a laser cavity (Ulrich *et al.*, 2006*a*).

Heavy ion beam pumping of gas lasers had first been demonstrated in 1983 at the Munich tandem van de Graaff accelerator by pumping an infrared He-Ar laser with a 100 MeV ^{32}S beam (Ulrich *et al.*, 1983). Investigations in this field were continued, but due to the limited pumping power densities, provided by ion accelerators, the wavelength range of the ion beam pumped lasers had been limited to the infrared and visible spectral region (Ulrich *et al.*, 1983, 1994). This situation has now been greatly improved due to the significant increase in beam intensity and beam quality available at the GSI ion accelerator facility.

The experiment described here is the first in a planned series dedicated to studying of short wavelength gas lasers using ion beam pumping. The projected parameter range for the next experiments in this series is discussed and detailed analytical and numerical estimations for the next two possible laser candidates are presented.

2. KrF* LASER EXPERIMENT

2.1. Ion Beam and Target Parameters

For a first demonstrational experiment, the well-known KrF* excimer laser line at a wavelength of 248 nm had been chosen. The selection of this wavelength was based on two main reasons: first, it is a rather short wavelength, already in ultraviolet (UV) region, and second, it is still easy to handle with respect to light detection. Radiation of this wavelength can propagate in air without significant attenuation. Therefore, there is no need to evacuate the light path between the laser setup and the detector as would be the case for vacuum ultraviolet (VUV) light with wavelengths below 200 nm. Light with a wavelength of 248 nm is also still in a range where usual quartz optics (diagnostic windows, lens, fibers, etc.) and charge-coupled device (CCD) detectors in cameras and spectrometers can be used.

The experiment was performed at the HHT target area at GSI in December 2005 (Ulrich *et al.*, 2006*a*, 2006*b*; Adonin *et al.*, 2007*a*). Pulses of uranium ions provided by the universal linear accelerator at GSI (UNILAC) were accumulated in the SIS-18 (heavy ion synchrotron at GSI) using the multi-multi-turn injection scheme (Spiller *et al.*, 2006). In the SIS-18, electron cooling was applied to the ion beam, which allowed to reduce the transverse and longitudinal emittance of the beam several times, which improved the focusing characteristics of the beam significantly (Steck *et al.*, 1993). Then the uranium ions were accelerated in the SIS ring to 250 MeV/u and compressed into one beam pulse with duration of about 110 ns (full width at half maximum (FWHM)) using adiabatic rebunching and fast bunch rotation techniques. After that, the ion beam was extracted and guided in the beam transport line to the HHT area and finally delivered to the laser cavity.

The beam pulses were applied as single pulses for quantitative measurements or with a repetition rate of up to about 0.1 Hz and reduced intensity for beam alignment, respectively. The intensity of the uranium beam pulses could be varied from about 10^8 to a maximum of 2.5×10^9 particles per pulse. Taking into account that the ions lost particle energy before entering the laser cell (see Section 2.3), the maximum pulse energy deposited by the ion beam in the laser gas was 6.7 J corresponding to a maximum beam power of about 61 MW.

The laser gas used in the experiment was a mixture of an excimer laser gas premix ($95.5\%Kr + 0.5\%F_2$) and a buffer gas (4.8%Ar). It was used in different mixing proportions:

35/65 and 60/40 of premix and buffer gas, respectively. The total gas pressure in the laser cell was varied between 1.2 and 2 bar.

2.2. Concept of the Experiment

The general concept of the experiment is demonstrated in Figure 1. The intense $^{238}U^{73+}$ beam pulse entered the laser cell from the right (Fig. 1) and was completely stopped in the laser gas. The position of the beam and the spot size of the beam right before entering the cell were observed with a gated CCD-camera looking at an Al_2O_3-scintillator installed on the beam axis. At a distance of approximately 30 cm behind the entrance point of the ions, the spontaneous emission from the laser gas was observed in a direction perpendicular to the ion beam axis through a sapphire viewport with a fast photodiode and a spectrometer (Fig. 1).

The pressure of the laser gas inside the cell was adjusted so that the ions would stop in a diagnostic cross-piece (Fig. 1) to make sure that they would not hit and damage the second laser mirror. The range of the ions was controlled by observing the Bragg-peak region with gated CCD-cameras installed in perpendicular directions in front of the cross-piece for beam diagnosing purposes (see next Section).

The stimulated emission along the ion beam axis was partially (less than 1%) decoupled from the cavity through the second mirror. To avoid saturation of the laser diagnostics, decoupled laser light was scattered off the rough surface of a sand-blasted Al-plate (Fig. 1) and then registered. By varying the distance between the laser diagnostics (photodiode and spectrometer) and the diffusely reflecting plate, it was possible to control the signal strength and thereby adjusting it to the dynamic range of optical diagnostics.

A He-Ne laser with 1 mm aperture (left item in Fig. 1) was installed and adjusted on the ion beam axis for a prealignment of the laser mirrors. This was possible because the exit (second) mirror had a dielectric coating on a quartz substrate and was therefore transparent for visible light whereas the entrance (first) mirror had an Al-coating that is reflective for visible light. A compact video camera installed in front of the laser aperture (Fig. 1) was used for visually controlling the reflected adjustment laser spots during remote alignment of the laser cavity with the He-Ne laser.

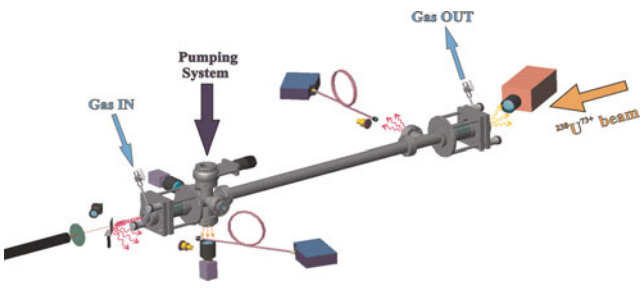

Fig. 1. (Color online) The general concept of the experiment (experimental setup with diagnostics).

2.3. Energy Losses of the Ions before Entering the Laser Cell

Before entering the laser cell, the ion beam had to traverse the following intermediate materials: an Al-window at the exit of the HHT-beamline (150 μm), a 210 cm long distance of ambient air, an Al_2O_3-scintillator (600 μm), an entrance foil for the laser cell made from stainless steel (50 μm), and, finally, the first laser mirror, mainly its SiO_2 substrate, 3.175 mm thick. Because of all these objects that could not be avoided in this test experiment, only the final 71 MeV/u of the particle energy were available to be deposited in the laser gas.

Table 1 lists the remaining energy of the ions and the increase of the beam radius and the ion's angular spread after propagation through each intermediate material between the exit of the beamline and the entrance of the laser cavity.

The calculations were performed using the SRIM and TRIM codes (from SRIM-2006 code package) for each intermediate material separately without taking ion beam straggling in the previous materials into account (Ziegler *et al.*, 2003). Each calculation used a statistics of 1000 ions and the results, listed in Table 1, are valid for 90% of the particles.

2.4. Shape of the Ion Beam inside the Laser Cell

One important point in the experiment was to determine the ion beam excited volume inside the laser cell. The stopping length of the ion beam in the laser gas could be determined by observing the position of the Bragg-peak region (see Section 3.3) and controlled by varying the gas pressure. The evolution of the diameter of the ion beam inside the laser cell could only be estimated using a simulation.

There are two effects that have influence on the spot size of the ion beam: beam transport and focusing in the HHT beamline and angular straggling due to scattering of the ion in front of and inside of the laser cell. These effects are independent from each other and can therefore be calculated separately.

The shape of the ion beam inside the cell, as defined by the final focusing system of the HHT-beamline (without taking interactions of ions with matter into account), were calculated using the beam transport simulation program for the HHT-line. The ion beam straggling due to ion-atom collisions in the intermediate materials as well as in the laser gas was calculated using the TRIM code (for an initially parallel beam with zero-diameter).

Combining beam focusing and straggling in the intermediate materials, it could be assumed that the ion beam was round with the diameter of 6.3 mm (FWHM) at the entrance to the laser cavity. The estimated beam diameter at the end of the ion range was 18.8 mm (FWHM) for the laser gas containing 40% Ar and 60% excimer laser premix.

Table 1. *Ion energy, increasing beam radius and angular spread after propagation of the ions through each intermediate material on their way to the laser cavity*

Traversed material/thickness		250 MeV/u (59.5 GeV)		
		Ion energy	Increase in beam radius	Angular spread of ions
Beamline exit Al-window	150 μm	58.52 GeV	54 nm	0.031°
Air gap	210 cm	50.84 GeV	1.7 mm	0.076°
Al_2O_3-scintillator	600 μm	44.24 GeV	0.63 μm	0.097°
SS-pressure window	50 μm	43.22 GeV	33 nm	0.057°
Entrance Quartz mirror	3.175 mm	16.89 GeV	8.3 μm	0.328°

A reliable measurement of the ion beam spot size was possible during the experiment only at the end of ion's range in the laser gas (Bragg-peak region). The measured value of the spot size of the beam was 16 mm (FWHM) for the case of the mixture: 40% of Ar and 60% of excimer laser premix, at a gas pressure of 1200 mbar, which is in good agreement with the estimated value of 18.8 mm.

3. EXPERIMENTAL SETUP AND DIAGNOSTICS

The laser setup consisted of a 1.2 m long stainless steel laser tube of 38 mm inner diameter, placed about 2 m behind the final focusing system of the beamline, vacuum system, high pressure gas filling system, mirror alignment units, and instrumentation for system control and optical diagnostics (Fig. 1).

3.1. Vacuum and High Pressure Gas System

A combination of an oil-free diaphragm roughing pump and a turbo-molecular pump had been used for the vacuum system (Fig. 1). During preparation of the experiment, the laser tube was baked at 130°C with a special heating wire. It was important to remove the water from the inner surface to avoid the formation of HF-acid during the experiment. A background pressure of 10^{-6} mbar was reached. During high pressure operation, the vacuum system was closed with a gate valve.

The high pressure gas system was connected to the laser cell at two points with 6 mm diameter Teflon tubes that are fluorine resistant and thick enough to allow pressures up to 10 bar to be used. To ensure a constant concentration of fluorine in the gas mixture and to prevent depletion of fluorine by reactions with impurities, a steady flow of the laser gas was established in the laser cell. The position of the connection points of the gas system to the laser cell was chosen in a way to maximize the volume inside the laser cell that was included in the gas flow (Fig. 1). Bottles containing the excimer-laser premix ($95.5\%Kr + 0.5\%F_2$) and pure Ar (4.8%) buffer gas, respectively, were connected to the system separately for preparing various mixing ratios. Laser gas inlet and outlet was remote controlled by a combination of an electro-mechanical valve actuator with a ball valve (gas inlet) and a metering valve with electrical motor on the outlet. This allowed remote control of the gas pressure and gas composition.

3.2. Optical Cavity

The optical resonator was formed by two mirrors. A first mirror was placed on the optical axis and traversed by the ion beam. It consisted of a flat, 25 mm diameter, 3.2 mm thick fused silica substrate with Al-MgF_2 coating. A second, dielectrically coated mirror, highly reflective for the laser wavelength of 248 nm was placed again on the optical axis at the other end of the laser cell. It had a 25 mm diameter, 6.35 mm thick plane-concave fused silica substrate with 3 m radius of curvature. The length of the optical cavity was 1.3 m. The second mirror was used as the output-coupler and used also as the window of the gas cell.

Each mirror had been mounted on an adjustment unit, specially constructed for high pressure (up to 10 bar) and precise alignment of the optical cavity. Each unit had two leveling screws that allowed adjusting the mirrors with micrometer step. Remote controlled electrical motors driving the leveling screws provided the possibility of on-line alignment during the experiment.

3.3. Diagnostics

Sapphire and MgF_2 viewports were installed at different places in the laser cell and were used as ultraviolet (UV)-transparent windows for optical diagnostics and spectrometry. The thickness of the optical material was chosen to withstand the pressure differentials up to 10 bar.

3.4. Laser Intensity and Time Shape

For measuring the time structure and intensity of the laser light (along the ion beam axis) as well as of the spontaneous light emission (perpendicular to the ion beam axis), two high speed, UV sensitive photodiodes were used. In order to register only the KrF* emission at a wavelength of 248 nm and block all other light emitted from the laser gas, each photodiode had been placed behind a bandpass interference

filter. The transmission band of these filters was 40 nm (FWHM) at a central wavelength of 254 nm (Hg-line).

The photodiodes were operated with a bias voltage of −117 V (separated from the power network). This gave a time resolution of better than 2 ns.

3.5. Spectral Measurements

Spectrally resolved measurements were performed with two compact spectrometers with fiber optics input and read-out *via* a USB-port. The spectrometers were installed at two different places to observe light emitted perpendicular to the laser axis (spontaneous emission) and along the laser axis (laser output), respectively. The light collecting optics was connected to the spectrometers *via* short (2 m length) UV-fibers. The spectrometers observed a wide wavelength range from 200 nm to 1100 nm with an optical resolution on the order of 2.3 nm. An electronic shutter used in spectrometers allows decreasing an integration time down to 10 μs.

3.6. Ion Beam Diagnostics

Ion beam diagnostics had been performed using the instrumentation installed at the HHT target station. The total number of particles in a beam pulse was recorded using a resonant current transformer installed in the extraction line from SIS-18. It has accuracy better than 2% (Reeg & Schneider, 2001). The time structure of the beam pulses was measured with a fast current transformer placed at the exit of the beamline. Its time resolution is better than 5 ns (Bergoz, 1991).

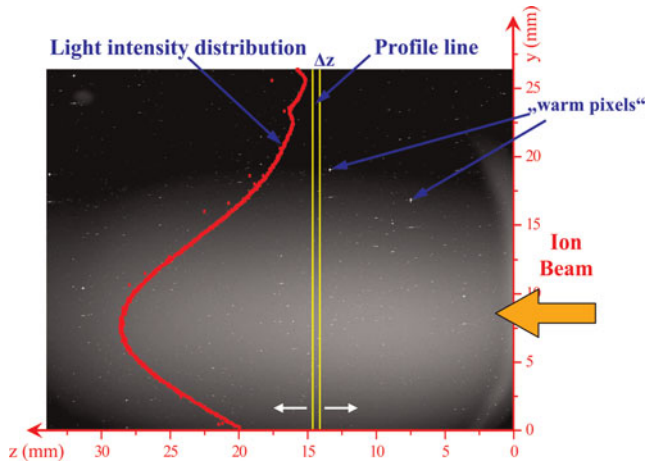

Fig. 2. (Color online) Example for a measurement of an intensity profile of fluorescent light emitted from the laser gas and recorded with a CCD-camera.

The beam spot size was observed at the entry of the laser gas cell with a 600 μm thick Al_2O_3-scintillator and near the exit of the cavity at the end of range of ions, using the gas fluorescence (Forck & Peters, 2004; Adonin *et al.*, 2005). The Al_2O_3-scintillator was used mostly for visually controlling the ion beam during the positioning and focusing

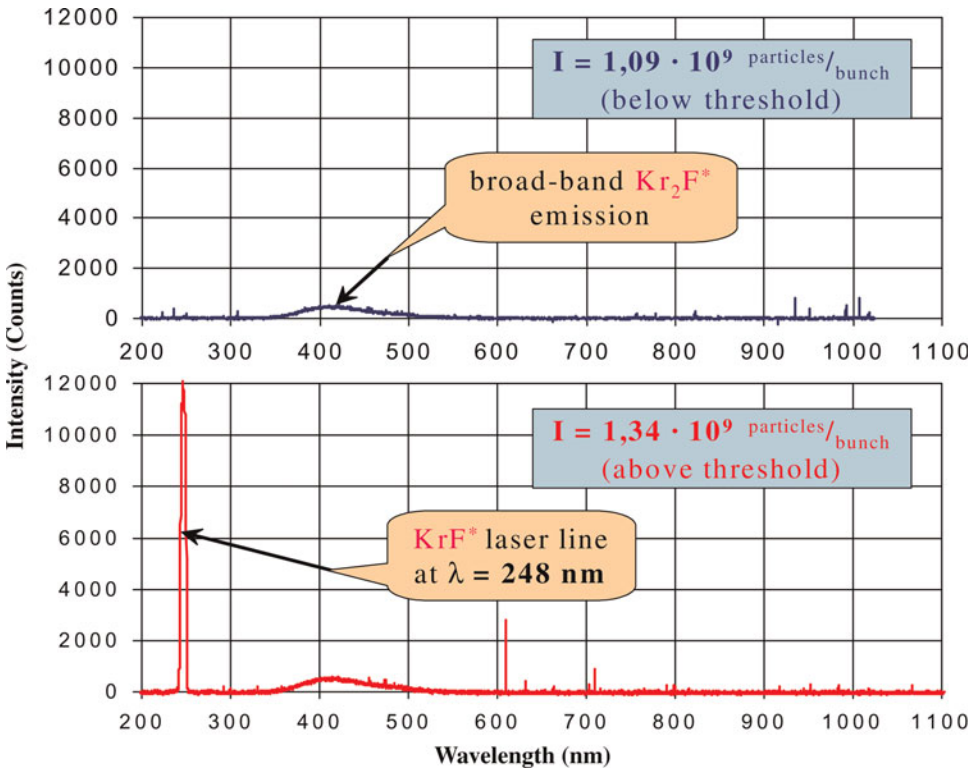

Fig. 3. (Color online) Indication of laser effect. On-axis spectra recorded for measurements with the beam intensities 1.09×10^9 (upper) and 1.34×10^9 (lower) part. per pulse are compared.

procedures. An estimation of the beam size at the end of range of the ions (in the Bragg-peak region) was performed with two compact high-resolution gated CCD-cameras installed in horizontal and vertical planes. The cameras registered fluorescent light emitted from the laser gas excited by the ion beam.

An example of an image showing fluorescent light recorded with the camera installed in the vertical plane is shown in Figure 2. The heavy ion beam comes from the right-hand side and is stopped in the field of view of the camera. The vertical profile line shows the light intensity distribution perpendicular to the ion beam axis (Fig. 2). The width of the profile Δz was optimized in order to reduce an influence of "warm pixels" (very bright points on the image consisting of 1 to 5 pixels, which appeared randomly due to hard background radiation in the experimental area induced by the high energy heavy ions). The horizontal profile (not shown in the figure) provides a measure of the distribution of light intensity along the beam axis allowing a localization of the Bragg-peak's maximum. The ion beam shape in the field of view of the camera could be obtained by scanning the image with vertical profiles line along the ion beam axis.

An analysis of the recorded images *via* light profiles provided information about the intensity distribution of the ion beam, beam position, beam envelope in observed region, the position of the Bragg-peak, and therefore also the range of ions. This in combination with gas pressure and gas composition provides *via* model programs for energy loss and range of the ions a value for the initial ion energy at the entrance of the laser cell.

4. RESULTS

4.1. Spectral Measurements

A first indication of the laser effect was obtained from the compact spectrometer, observing light emission along the ion beam axis. As soon as the ion beam intensity became higher than a certain value, strong laser emission on the line at $\lambda = 248$ nm appeared in the spectrum (Ulrich *et al.*, 2006*a*, 2006*b*; Adonin *et al.*, 2007*a*). This indicated that the pumping power density provided by the ion beam exceeded the power level necessary to reach the laser threshold in the optical cavity. Examples of on-axis spectra for beam intensities of 1.09×10^9 (below the threshold) and 1.34×10^9 (above the threshold) particles per bunch are shown in Figure 3. The intensity of broad-band emission of Kr_2F^* (in visible and soft UV spectral range) increased linearly with the ion beam intensity. It is important to note

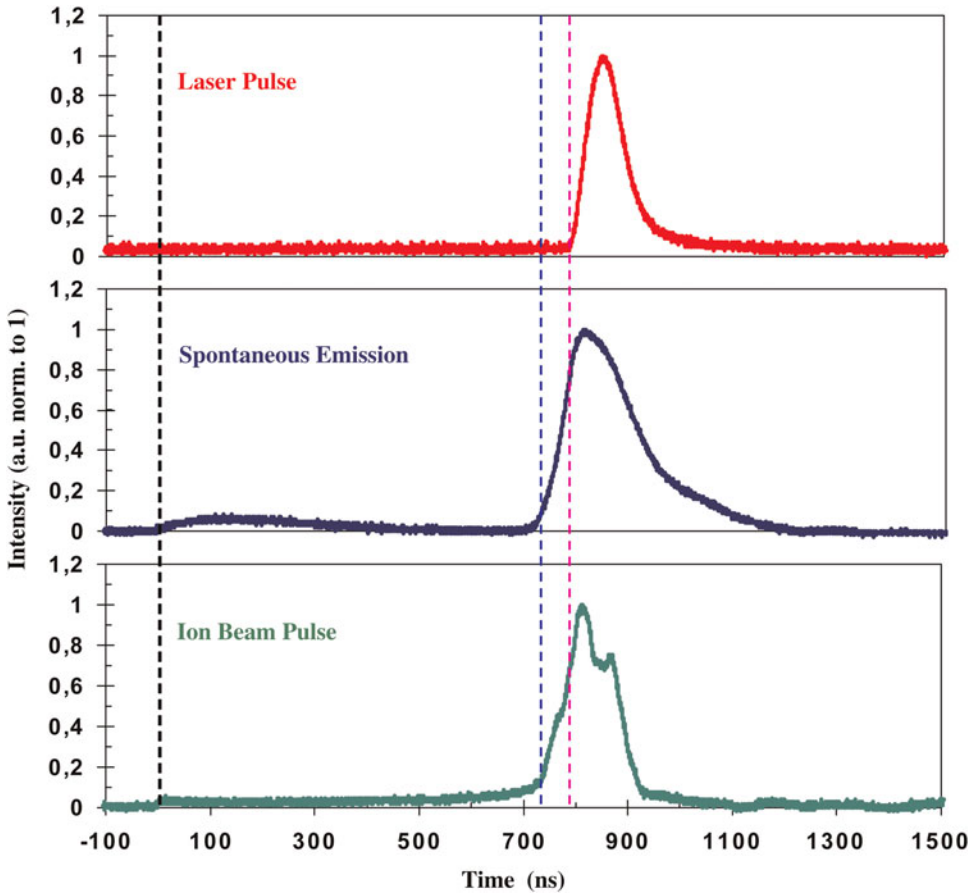

Fig. 4. (Color online) Time structure of the ion beam pulse, spontaneous and stimulated emissions.

that, the exit cavity mirror was transparent for visible light and nearly 100% (>99.8%) reflective for 248 nm light. Therefore, only a small fraction of the laser or spontaneously emitted light at this wavelength could be decoupled from the cavity and registered. This is the reason why the spontaneous emission at 248 nm is not seen on the upper spectrum.

Line narrowing, another feature characteristic for laser light in comparison with just spontaneous emission, has also been observed during the experiment. Spectra of spontaneous emission from the laser gas (observed perpendicularly to the beam axis) as well as laser output spectra were recorded with the same spectrometer. By comparing both spectra, a clear difference was found between the widths of the KrF* line ($\lambda = 248$ nm) in on-axis spectra and spectra recorded at 90° with respect to the optical axis (Adonin *et al.*, 2007*a*). The effect is clearly visible but due to the relatively low spectral resolution of the spectrometer of 2.3 nm not very pronounced.

4.2. Time Structure and Characteristics

Another proof of the laser effect is based on the different time structures of spontaneous and stimulated emission observed with the photodiodes (Ulrich *et al.*, 2006*a*). Spontaneous emission lasts about 40 ns longer than the ion beam pulse, which means that afterglow processes in the laser gas play a considerable role. The rising edge of the spontaneous emission has the same steepness as the leading edge of the ion beam pulse. The duration of the laser output pulse, however, is shorter than the ion beam pulse and its rising edge is steeper (Fig. 4).

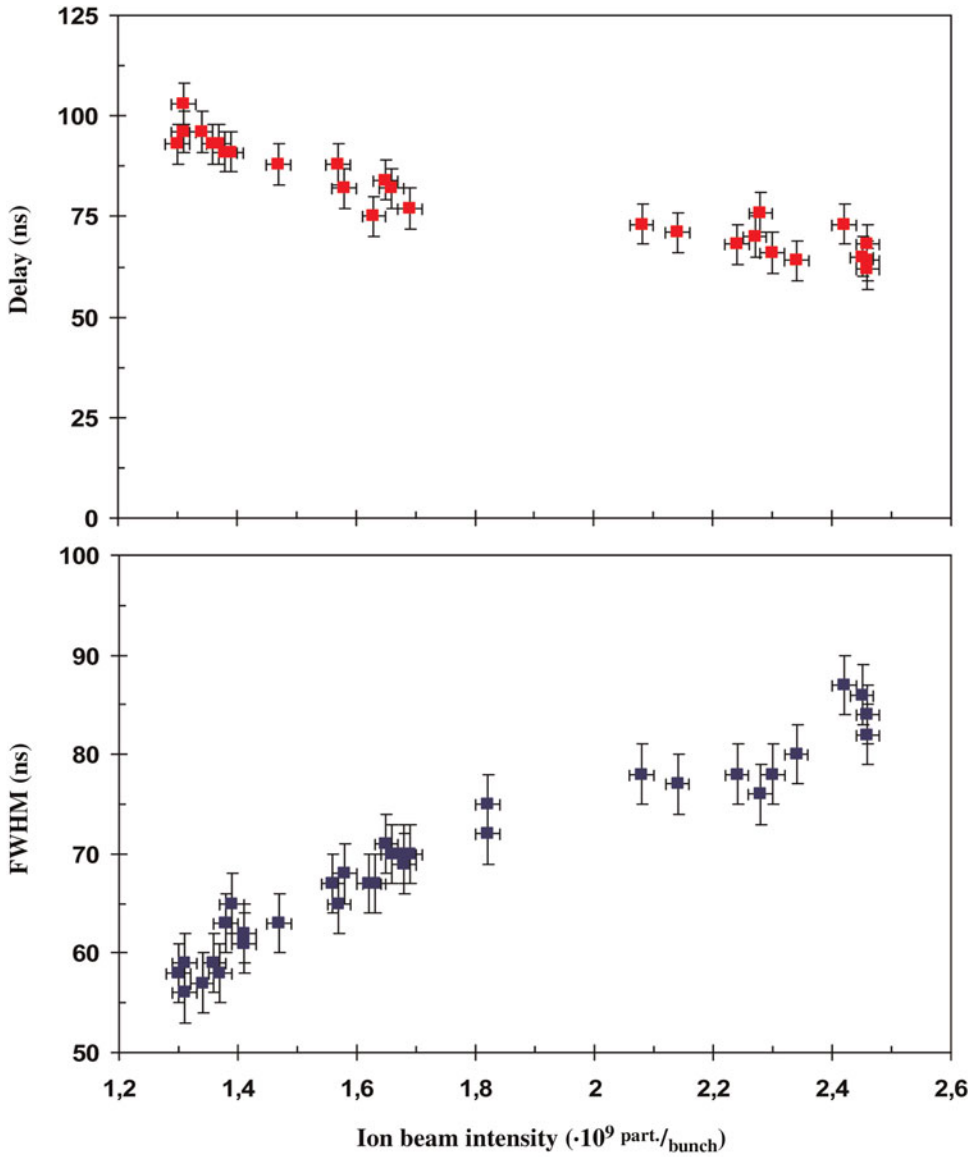

Fig. 5. (Color online) The delay (upper) and the duration (lower) of the laser emission as a function of the beam intensity.

The time structure of the ion beam pulse, registered with the fast current transformer, as well as the structures of spontaneous and laser emissions are shown in Figure 4. Maximum amplitudes of signals were normalized to unity in order to provide a better comparison of the structure. The ion beam pulse had a complex time structure with two maxima, long tails (at the beginning and at the end), and a low intensity pre-pulse at the beginning. This is due to the limited synchronization between the beam bunch rotating in the SIS ring and a so called kicker magnet that extracts the ions into the beam transfer line. It is interesting to note that the ion beam pre-pulse was also observed with comparatively high intensity in the spontaneous emission. This indicates a non-linear dependence of light emission from power density deposited in the gas. It also allowed us to associate the signals from the FCT and from the side photodiode precisely in time since the spontaneous emission starts instantaneously with the ion beam pre-pulse.

Above laser threshold an increase of laser pulse duration with increasing pumping power as well as a dependence of the delay time of the onset of laser emission with respect to the onset of the pumping pulse has been observed as a function of the beam intensity. Figure 5 shows the dependence of laser pulse duration (signal from the on-axis photodiode) from ion beam intensity. This dependence is non-linear and converges to a certain limit with increasing beam intensity. Here, it is important to note that the ion beam pulse duration was around 110 ns for all shots, independent of the number of particles in the pulse. The duration of the laser pulse varied from 56 ns near laser threshold and 87 ns for pumping pulses with the maximum intensity of 2.46×10^9 particles per bunch. The experimental error of

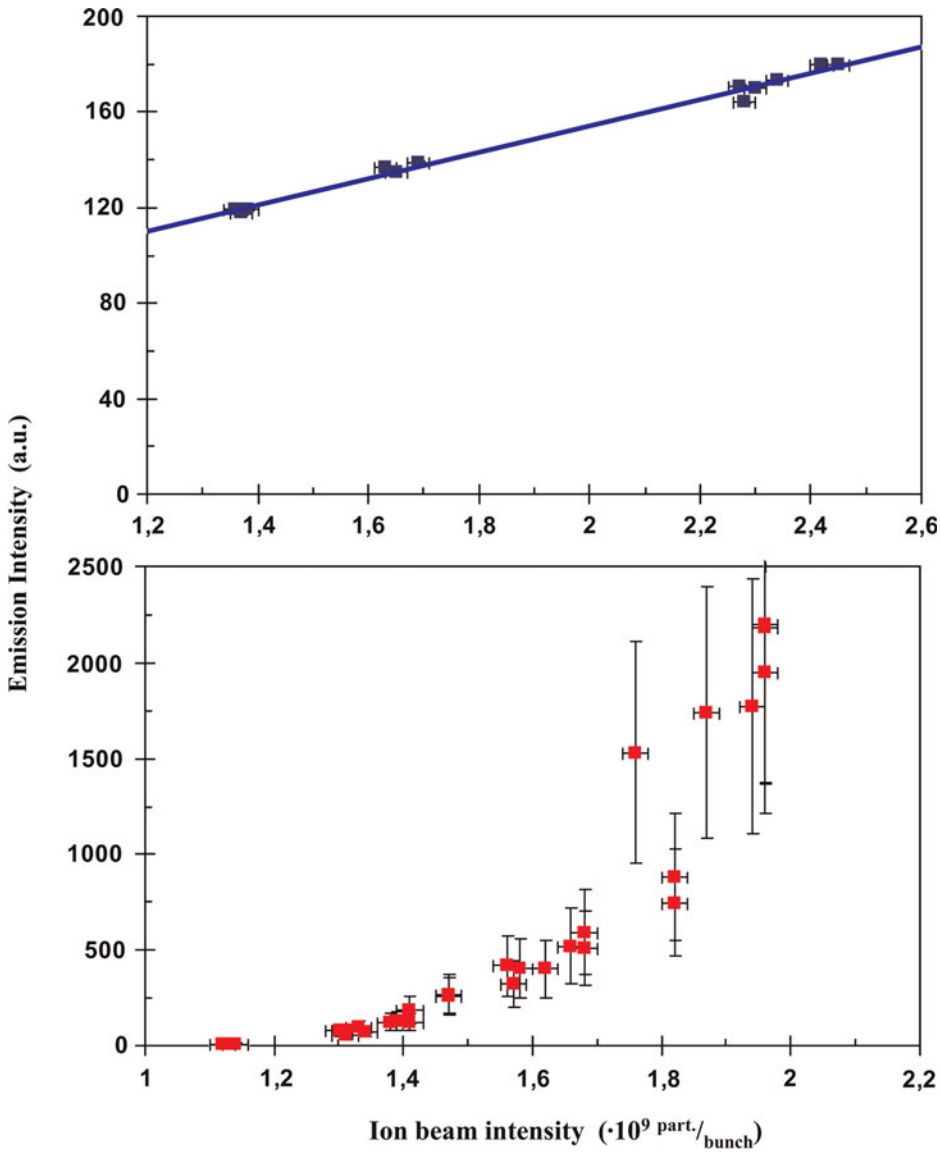

Fig. 6. (Color online) The behaviour of the spontaneous and the laser emission with increasing of the ion beam intensity.

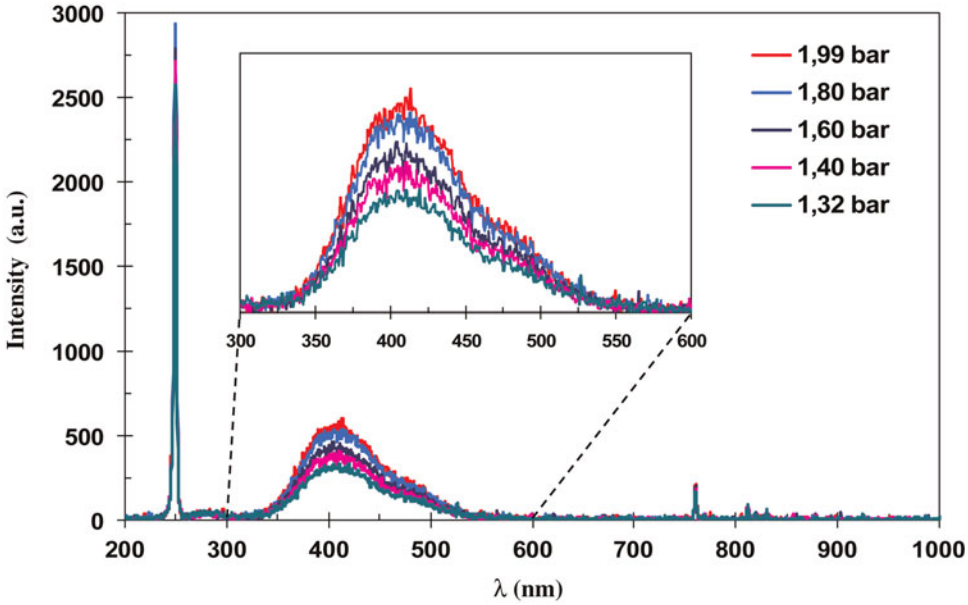

Fig. 7. (Color online) Spectra of the spontaneous emission at different gas pressures.

the pulse width measurements is on the order of ± 3 ns. The duration of the spontaneous light emission did not depend on the ion beam intensity and was on the order of 150 ns (FWHM).

The delay of the onset of laser emission decreased with increasing ion beam power (number of particles in the pulse). It was about 100 ns (± 5 ns) for beam intensities slightly above laser threshold and decreased to 65 ns (± 5 ns) for maximum available beam intensity (see Fig. 5).

4.3. Laser Intensity

The dependences of spontaneous and stimulated emission intensity from pumping power were measured, again showing clear indication of laser effect. In Figure 6, the intensity of on-axis and off-axis light emission is shown as a function of the number of particles in the ion beam pulses.

In the case of spontaneous emission (off-axis), the experimental points show a linear dependence from beam intensity. This indicates, for example, that within the intensity range and for the target parameters used here, no hydrodynamical effects lead to appreciable changes in gas emissivity and gas transparency. The linear regression starts from a certain value (not from zero-point), this could be explained by the presence of the nuclear and radiation background registered by the photodiodes during the measurements.

In contrast to spontaneous emission, the laser emission has a non-linear dependence of the light output with respect to ion beam intensity and therefore on energy deposited in the gas (Fig. 6). First of all, this dependence has threshold behavior, which is a clear indication of the laser effect. The value of the laser threshold, estimated from the photodiode data, is 1.2×10^9 particles per bunch. Theoretically, this dependence can be expected to be a superposition of an exponential growth at the beginning (right above threshold) and a linear dependence, starting from some value for ion beam intensity, where the saturation of laser intensity is reached.

4.4. Pressure Dependence

Within the course of the experiments, the dependence of spontaneous emission spectra on gas pressure was measured in a range from 1.3 to 2 bar (Adonin *et al.*, 2007*b*). The spectrum of spontaneously emitted light from the laser gas contains three main components: emission of the KrF* band at $\lambda = 248$ nm (laser transition), broad-band emission of Kr_2F^* molecules in a wide region from $\lambda = 350$ to 550 nm, and atomic lines of Ar-I and Kr-I in the region $\lambda > 750$ nm (see Fig. 7). The KrF* emission has the highest peak amplitude, more than 80% of total light intensity can be attributed to broad-band Kr_2F^* emission. Atomic lines of Ar-I and Kr-I have a two orders of magnitude lower integral intensity than Kr_2F^*. It was found that the optimum for laser experiments in the sense of laser efficiency is the lowest gas pressure in the region which has been studied (Adonin *et al.*, 2007*b*).

5. CONCLUSIONS

The main result of this work performed at GSI accelerator facility is that a heavy ion beam pumped UV laser has been successfully demonstrated for the first time using the well-known laser transition of $\lambda = 248$ nm KrF* excimer laser. The pumping power required to reach laser threshold for this specific setup was 0.51 MW/cm^3, which corresponds to an ion beam intensity of 1.2×10^9 particles per pulse.

The laser effect had been verified by several independent methods, listed below: (1) appearance of the laser line, (2) spectral narrowing of the laser transition, (3) temporal narrowing of light emission on the laser line, (4) non-linear dependence of laser output from pumping power, (5) correlation of laser effect with cavity alignment.

By a calibration of the photodiode detectors using a commercial KrF* excimer laser with known laser parameters used in the same geometry as in the accelerator experiment made provided a total energy of the laser pulse obtained in the heavy ion pumping experiment: ≈2 mJ for an ion beam intensity of 2×10^9 particles per pulse. Maximum laser output power, corresponding to the same beam intensity was about 20 kW. The total energy deposited by the ion beam in the laser gas for this beam intensity was about 5.3 J. From these values a conversion efficiency of ion beam energy to the laser light of 0.04% has been derived. Note, that the experiment was designed to reach the laser threshold and not to optimize the output power.

For the case of a half-symmetric optical resonator, as was used in the experiment, the calculated spot sizes of the laser beam inside the optical cavity (Siegman, 1986) were 0.34 mm on the flat mirror (laser beam waist) and 0.46 mm on the curved mirror (maximum spot size). Comparing the total beam excited volume (see Section 2.4) with the mode volume of the optical resonator shows that only a small fraction of the beam excited laser gas could contribute to the laser output. This is one of the reasons of relatively low conversion efficiency besides e.g., the unfavorable mirror reflectivities.

As a general conclusion of the present work, it could be shown that the intensity, space and time characteristics of ion beams, provided by the heavy-ion synchrotron SIS-18 at GSI are now sufficient to pump gas lasers in the UV spectral region.

6. PERSPECTIVES FOR FUTURE EXPERIMENTS

As a next step in studying short wavelength lasers pumped with heavy ion beams, it is planned to reduce the laser wavelength down to the VUV spectral range ($\lambda < 200$ nm) and to proceed to the excimer lasers of the pure rare gases. The second continua of rare gas excimer will be used as a laser transition: Xe_2^* ($\lambda = 173$ nm), Kr_2^* ($\lambda = 146$ nm), Ar_2^* ($\lambda = 126$ nm), and maybe Ne_2^* ($\lambda = 83$ nm) and He_2^* ($\lambda = 80$ nm). The advantage of these systems is that the pure rare gases are technically easier to handle and reduce the safety issues of the experiment. However, these lasers require considerably higher pumping power levels in comparison with KrF* excimer laser, because of the shorter wavelength and significantly broader laser transition.

6.1. Increasing of the Pumping Power

The pumping power required to reach a certain gain level to overcome the losses at the laser threshold is proportional to the width of the laser transition ($\Delta\lambda$) and inversely proportional to the fourth power of the laser wavelength (λ^4) (Siegman, 1986). Therefore, to achieve the same optical gain, for example, in the case of Xe_2^* excimer ($\lambda = 172$ nm; $\Delta\lambda \approx 15$ nm), it will require roughly 30 times higher pumping power than in the case of KrF* excimer ($\lambda = 248$ nm; $\Delta\lambda \approx 2$ nm).

In the case of heavy ion beam pumping, there are several ways to increase the pumping power density in the laser medium: (1) using higher Z ion species (in our case, we have used $^{238}U^{92}$, the highest Z available at GSI), (2) increasing the number of particles per beam pulse (the maximum intensity for uncooled U-beam obtained at GSI was 4×10^9 particles per pulse (Varentsov *et al.*, 2004)), (3) compressing the ion beam pulse in time (with existed technique at GSI the bunch compression of the ion beam achieved a best value of 100 ns FWHM), (4) reducing the beam spot size of the ion beam inside the laser cell

Since for the first three points, we are near the existed limit, the only way to increase the pumping power density is to reduce the ion beam excited area in the laser medium. The experience of the previous experiment has shown that one of the key problems of heavy-ion-beam pumping is the significant beam straggling in the laser gas cell. This is due to the ions scattering in the laser gas as well as in the intermediate materials between the beamline and the gas cell. As one can see from Table 1, the main contribution to the angular spread of the ion beam before entering the cavity was due to the long (more than 2 m) air section and the thick (3.2 mm) quartz mirror. We can reduce the angular spread of the ion beam at the cavity entrance and therefore the beam straggling by decreasing the air gap and the thickness of the entrance cavity mirror. With the present setup, it is possible to reduce the air section down to 20 cm without any changes in the design. A thin (1.5 mm) Si-wafer can be used as a substrate for the entrance mirror. Also the scintillator at the entrance of the laser cell can be removed since it is not used during the measurements.

To reduce the ion beam straggling inside the laser cell more, one can proceed to shorter resonator length (shorter beam stopping length), and higher initial ions energy. Let us consider a new length of the optical resonator of 60 cm. In order to pump more energy in the laser gas as well as to decrease the energy loss of the ions in the intermediate materials (and, consequently, to reduce the angular spread of the ion beam at cavity entry), the initial energy of the ions can be increased and we consider cases with 300 and 350 MeV/u, respectively. The consequences of these measures with respect to gas pressure will be discussed in the next paragraph.

In Table 2, the energy of U-ions as well as the increase of the ion beam radius after propagation through certain intermediate material on the way to the cavity is shown. Calculations were performed using the SRIM-2006 code package for initial ion energies of 300 and 350 MeV/u.

Table 2. *Ions energy and increasing of the beam radius in the intermediate materials between the beamline and the laser cavity with improved setup*

Propagated material	Thickness	Ion energy after propagation (GeV)		Blowing of the ion beam (for 90% of particles)	
Initial ions energy		71.4 (300 MeV/u)	83.3 (350 MeV/u)	71.4 (300 MeV/u)	83.3 (350 MeV/u)
Exit Al-window from the beamline	150 μm	70.51	82.47	50 nm	46 nm
Air gap	20 cm	69.87	81.87	44 μm	40 μm
Stainless steel pressure window	50 μm	69.06	81.13	27 nm	23 nm
Cavity mirror on Si-wafer	1.5 mm	61.05	73.71	2 μm	1.7 μm

As shown in Table 2, the part of the initial ion energy that will be deposited in the laser gas is 61.05 and 73.71 GeV for the cases of 300 and 350 MeV/u, respectively. This is roughly 3.6 and 4.4 times higher than in the case of the first experiment (Table 1). The expected expansion of the ion beam due to ion scattering is sufficiently smaller than before.

6.2. Pressure Requirements

The shorter length of the optical resonator will require higher gas pressures inside the laser cell in order to stop the ion beam in the laser gas. Therefore, the minimum gas pressures required for the experiments with various rare gases are as follows:

	Xe	Kr	Ar	Ne
300 MeV/u	6.5 bar	9.3 bar	17 bar	29 bar
350 MeV/u	8.6 bar	12.4 bar	22.7 bar	39 bar

The present setup can be used with gas pressures up to 10 bar. This limit is defined by the mirror adjustment units of the laser cavity. It is planned to use the optical cavity only in experiments with Xe and Kr excimers for the wavelengths of 173 and 146 nm, respectively. With the other gases, it is planned to operate the laser in amplified spontaneous emission mode, therefore, the pressure limit of the present setup is actual only for the cases of Xe and Kr gases.

6.3. Calculations for Xe- and Kr- Cases

Since Xe and Kr are the most appropriate candidates as the laser medium for the next experiments, we consider two cases (variants) for further calculations:

Laser gas	Laser wavelength	Gas pressure	Initial ions energy	Beam stopping length	Resonator length
Xe	172 nm	8.6 bar	350 MeV/u	60 cm	70 cm
Kr	146 nm	9.3 bar	300 MeV/u	60 cm	70 cm

Experiments with parameters listed above do not require significant changes in the present setup.

The expected diameters of the ion beam inside the cavity (taking focusing parameters and beam straggling into account) could be as follows: 2.2 mm (FWHM) at the cavity entrance and 9.8 mm and 8.7 mm (FWHM) in the Bragg-peak region for Xe and Kr, respectively. These diameters are considerably smaller than the beam diameters in the previous experiment (6 mm at the entrance and around 15 mm near the Bragg-peak).

Assuming a maximum intensity of the ion beam of 4×10^9 particles per pulse (Varentsov *et al.*, 2004), the projected average energy density deposited in the laser gas along the beam axis is: 4.1 J/cm^3 and 4.08 J/cm ^{3} for Xe and Kr, respectively. This corresponds to 41 MW/cm^3 and 40.8 MW/cm^3 peak power densities for the 100 ns (FWHM) ion beam pulses. These values are more than 30 times higher than the maximum value of deposited power density of 1.1 MW/cm^3 achieved in the first experiment.

Assuming an efficiency of the upper state population ε_{up} of 10% (Hutchinson, 1980; Sakurai *et al.*, 1987) the part of the energy deposited in the gas that produces a certain number of excimer molecules per unit time and volume is: 4,1 MJ/s·cm^3 and 4,08 MJ/s·cm^3 for Xe and Kr cases, respectively.

$$R_{lu} = \frac{p_{pd}}{E_{ion}} \cdot \varepsilon_{up}$$

The ionization energies of xenon and krypton atoms are 12 eV and 14 eV, respectively. From these values the pumping rate R_{lu} (number of upper states produced in a volume per unit time) could be calculated: with $R_{lu} = 2.14 \times 10^{24}$ s^{-1}·cm^{-3} for Xe and $R_{lu} = 1.82 \times 10^{24}$ s^{-1}·cm^{-3} for Kr. Since the lifetime of the excimer states are: 5.5 ns for Xe_2^* (Keto *et al.*, 1974) and around 6 ns for Kr_2^*, respectively (Koehler *et al.*, 1975; Smirnov, 1983), the spontaneous emission rates will be: 1.82×10^8 s^{-1} and 1.67×10^8 s^{-1} for Xe and Kr cases, respectively.

Assuming that the quenching of the excited states occurs every collision with an atom or a molecule, the quenching rate will be equal to the average collision frequency ν_{coll}, which in turn is defined by the average velocity $<\upsilon>$ and

the mean free path L_{free} of the particles:

$$\nu_{coll} = \frac{< v >}{L_{free}}.$$

The average velocity for room temperature is 238 m/s and 298 m/s, and the mean free path is approximately 0.52 μm and 0.56 μm for Xe and Kr, respectively. Thus, the estimated in this way collisional quenching rate is 4.6×10^8 s^{-1} and 5.3×10^8 s^{-1} for Xe and Kr cases, respectively.

Thereby, the upper state population N_u in the case of Xe will be 3.33×10^{15} molecules per cm^3 and in case of Kr – 2.61×10^{15} molecules per cm^3, calculated by the following formula:

$$N_u = \frac{R_{lu}}{A_{ul} + B_{ul} + C_{ul}}.$$

The stimulated emission cross-section σ_{st} for Xe_2^* is assumed to be $1.5 \times 10^{17} cm^2$ and for Kr_2^* it can be estimated around 10^{17} cm^2 (Hutchinson, 1980). The photons emitted by Xe_2^* as well as by Kr_2^* molecules have sufficient energy to ionize other excimer molecules (Xe_2^* and Kr_2^*, respectively), thereby reducing the gain of the laser. The cross-section of this photoionization process is estimated to be 2×10^{-18} cm^2 for Xe_2^* and around 10^{-18} cm^2 for Kr_2^* (Hutchinson, 1980; Eckstrom *et al.*, 1988). Thus, by taking into account the photoionization as a competitive process to the stimulated emission, the small signal gain g_{ss} is predicted to be about 4.3% per cm and about 2.3% per cm for Xe and Kr cases, respectively.

Assuming the length of the active medium in the resonator of 60 cm (range of the ions in the laser gas) for both cases, and using the highly reflective cavity mirrors with reflectivity of 96% for $\lambda = 172$ nm (Xe case) (Eckstrom *et al.*, 1988), and about 85% for $\lambda = 146$ nm (Kr case) (Sasaki *et al.*, 2001), a net gain per single pass factor of 2.54 for the Xe_2^* and 1.22 for the Kr_2^*, respectively, can be obtained. Since for a 100 ns pumping pulse, one can assume around 42 single trips, the clear laser action can be expected for both cases.

7. OUTLOOK

The use of heavy ion beams as a pumping source may lead to new pumping schemes beyond the known excimer systems based on energetically higher lying levels and transition energies, and thereby considerably shorter wavelengths (in the extreme UV and X-ray spectral region). This may be achieved *via* the high cross-sections for multiple-ionization of the target species. In the framework of the future facility for antiprotons and ion research named FAIR project, it is planned to upgrade the existing accelerators at GSI and build up a new heavy ion synchrotron that will be composed of two rings: SIS-100 and SIS-300. It is expected that FAIR facility will provide the beams of heavy ions that exceed the current beam parameters up to two orders of magnitude by intensity and three orders by the beam power. Thus, it opens wide perspectives for studying short wavelength lasers and for discovering new laser schemes which could be efficiently pumped only with intense heavy ion beams.

REFERENCES

Adonin, A., Hoffmann, D.H.H., Jacoby, J., Kulish, M., Ni, P., Nikolaev, D., Shilkin, N., Spiller, P., Udrea, S. & Varentsov, D. (2005). Measurements of heavy ion beam profiles in gases. Plasma Physics Annual Report 2004. Darmstadt, Germany: GSI.

Adonin, A., Jacoby, J., Turtikov, V., Fertman, A., Golubev, A., Hoffmann, D.H.H., Ulrich, A., Varentsov, D. & Wieser, J. (2007*a*). Laser effect on the 248 nm KrF transition using heavy ion beam pumping. *Nucl. Instr. Meth. A* **577**, 357–360.

Adonin, A., Jacoby, J., Turtikov, V., Fertman, A., Golubev, A., Hoffmann, D.H.H., Ulrich, A., Varentsov, D. & Wieser, J. (2007*b*). Pressure dependence of excimer emission induced by an intense uranium beam. Scientific Report 2006. Darmstadt, Germany: GSI.

Bergoz, J. (1991). Handbook for fast current transformer for heavy ion fusion at GSI. Technical Report. Darmstadt, Germany: GSI.

Brau, Ch.A. (1984). Rare gas halogen excimers. In *Excimer Lasers* (Ch. K. Rhodes, Ed.). New York: Springer-Verlag.

Eckstrom, D.J., Nakano, H.H., Lorents, C.C., Rothem, T., Betts, J.A., Lainhart, M.E., Dakin, D.A. & Maenchen, J.E. (1988). Characteristics of electron-beam-excited Xe_2^* at low pressures as a vacuum ultraviolet source. *J. Appl. Phys.* **64**, 1679–1690.

Forck, P. & Peters, A. (2004). Methods of beam profile measurements at high current hadron accelerators. *Proc ICFA-HB 2004*. Bensheim, Germany.

Hoffmann, D.H.H., Blazevic, A., Ni, P., Rosmej, O., Roth, M., Tahir, N.A., Tauschwitz, A., Udrea, S., Varentsov, D., Weirich, K. & Maron, Y. (2005). Present and future perspectives for high energy density physics with intense heavy ion and laser beams. *Laser Part. Beams* **23**, 47–53.

Hutchinson, M.H.R. (1980). Excimers and excimer lasers. *Appl. Phys.* **21**, 95–114.

Jacoby, J., Hoffmann, D.H.H., Laux, W., Müller, R.W., Wahl, H., Weyrich, K., Boggasch, E., Heimrich, B., Stöckl, C. & Wetzler, H. (1995). Stopping of Heavy Ions in a Hydrogen Plasma. *Phys. Rev. Lett.* **74**, 1550–1553.

Jacoby, J., Hoffmann, D.H.H., Müller, R.W., Mahrt-Olt, K., Arnold, R.C., Schneider, V. & Maruhn, J. (1990). Hydrodynamic motion of a heavy-ion-beam-heated plasma. *Phys. Rev. Lett.* **65**, 2007–2010.

Karelin, A.V., Sinyanskii, A.A. & Yakovlenko, S.I. (1997). Nuclear-pumped lasers and physical problems in constructing a reactor-laser. *Quant. Electr.* **27**, 375–402.

Keto, J.W., Gleason, R.E., Jr. & Walters, G.K. (1974). Production mechanisms and radiative lifetimes of argon and xenon molecules emitting in the ultraviolet. *Phys. Rev. Lett.* **33**, 1365–1368.

Koehler, H.A., Ferderber, L.J., Redhead, D.L. & Ebert, P.J. (1975). Vacuum-ultraviolet emission from high-pressure krypton. *Phys. Rev. A* **12**, 968–973.

Kuehl, T., Ursescu, D., Bagnoud, V., Javorkova, D., Rosmej, O., Cassou, K., Kazamias, S., Klisnick, A., Ros, D., Nickles, P., Zielbauer, B., Dunn, J., Neumayer, P., Pert, G. & Team, P. (2007). Optimization of the non-normal incidence, transient pumped plasma X-ray laser for laser spectroscopy and plasma diagnostics at the facility for antiproton and ion research (FAIR). *Laser Part. Beams* **25**, 93–97.

Neumayer, P., Bock, R., Borneis, S., Brambrink, E., Brand, H., Caird, J., Campbell, E.M., Gaul, E., Goette, S., Haefner, C., Hahn, T., Heuck, H.M., Hoffmann, D.H.H., Javorkova, D., Kluge, H.J., Kuehl, T., Kunzer, S., Merz, T., Onkels, E., Perry, M.D., Reemts, D., Roth, M., Samek, S., Schaumann, G., Schrader, F., Seelig, W., Tauschwitz, A., Thiel, R., Ursescu, D., Wiewior, P., Wittrock, U. & Zielbauer, B. (2005). Status of PHELIX laser and first experiments. *Laser Part. Beams* **23**, 385–389.

Reeg, N. & Schneider, N. (2001). Current transformers for GSI's keV/u to GeV/u ion beams. *DIPAC Proc. ESRF*. Grenoble, France.

Rocca, J.J., Shlyaptsev, V., Tomasel, F.G., Cortazar, O.D., Hartshorn, D. & Chilla, J.L.A. (1994). Demonstration of a discharge pumped table-top soft-X-ray laser. *Phys. Rev. Lett.* **73**, 2192–2195.

Sakurai, T., Goto, N. & Webb, C.E. (1987). Kr_2^* excimer emission from multi-atmosphere discharges in Kr, Kr-He and Kr-Ne mixtures. *J. Phys. D: Appl. Phys.* **20**, 709–713.

Sasaki, W., Shirai, T., Kubodera, S., Kawanaka, J. & Igarashi, T. (2001). Observation of vacuum-ultraviolet Kr_2^* laser oscillation pumped by a compact discharge device. *Opt. Lett.* **26**, 503–505.

Siegman, A.E. (1986). *Lasers*. Sausalito, CA: University Science Books.

Smirnov, B.M. (1983). Excimer molecules. *Sov. Phys. Uspekhi* **26**, 31–58.

Spiller, P., Blasche, K., Blell, U., Forck, P., Klingbeil, H., Franchetti, G., Franczak, B., Omet, C., Kirk, M., Peters, A., Reich, H., Ramakers, H., Redelbach, A., Scheeler, U. & Schütt, P. (2006, Aug.). SIS18 Status Report. GSI Report 2006–1. GSI: Darmstadt, Germany.

Steck, M., Beckert, K., Eickhoff, H., Franzke, B., Nolden, F. & Spadtke, P. (1993). Electron cooling of heavy ions at GSI. *Proc. PAC 93*. Washington, DC.

Sullivan, J.A. (1987). Design of a 100-kJ KrF power amplifier module. *Fusion Techn.* **11**, 684–704.

Sullivan, J.A., Allen, G.R., Berggren, R.R., Czuchlewski, S.J., Harris, D.B., Jones, M.E., Krohn, B.J., Kurnit, N.A., Leland, W.T., Mansfield, C., McLeod, J., McCown, A.W., Pendergrass, J.H., Rose, E.A., Rosocha, L.A. & Thomas, V.A. (1993). KrF amplifier design issues and application to inertial confinement fusion system design. *Laser Part. Beams* **11**, 359–383.

Tahir, N.A., Adonin, A., Deutsch, C., Fortov, V.E., Grandjouan, N., Geil, B., Grayaznov, V., Hoffmann, D.H.H., Kulish, M., Lomonosov, I.V., Mintsev, V., Ni, P., Nikolaev, D., Piriz, A.R., Shilkin, N., Spiller, P., Shutov, A., Temporal, M., Ternovoi, V., Udrea, S. & Varentsov, D. (2005). Studies of heavy ion induced high-energy-density states in matter at the GSI Darmstadt SIS-18 and future FAIR facility. *Nucl. Instr. Meth. A* **544**, 16–26.

Tahir, N.A., Kim, V., Matvechev, A., Ostrik, A., Lomonosov, I.V., Piriz, A.R., Cela, J.J.L. & Hoffmann, D.H.H. (2007). Numerical modeling of heavy ion induced stress waves in solid targets. *Laser Part. Beams* **25**, 523–540.

Tahir, N.A., Schmidt, R., Brugger, M., Lomonosov, I.V., Shutov, A., Piriz, A.R., Udrea, S., Hoffmann, D.H.H. & Deutsch, C. (2007). Prospects of high energy, density physics research using the CERN super proton synchrotron (SPS). *Laser Part. Beams* **25**, 639–647.

Ulrich, A., Adonin, A., Jacoby, J., Turtikov, V., Fernengel, D., Fertman, A., Golubev, A., Hoffmann, D.H.H., Hug, A., Krücken, R., Kulish, M., Menzel, J., Morozov, A., Ni, P., Nikolaev, D.N., Shilkin, N.S., Ternovoi, V.Ya., Udrea, S., Varentsov, D. & Wieser, J. (2006*a*). Excimer laser pumped by an intense, high-energy heavy-ion beam. *Phys. Rev. Lett.* **97**, 153901.

Ulrich, A., Adonin, A., Jacoby, J., Turtikov, V., Fernengel, D., Fertman, A., Golubev, A., Hoffmann, D.H.H., Hug, A., Krücken, R., Kulish, M., Menzel, J., Ni, P., Sharkov, B., Udrea, S., Varentsov, D., Wahl, H. & Wieser, J. (2006*b*). Heavy-ion-beam pumped excimerlaser. Scientific Report 2005. GSI: Darmstadt, Germany.

Ulrich, A., Bohn, H., Kienle, P. & Perlow, G.J. (1983). Heavy ion beam pumped He-Ar laser. *Appl. Phys. Lett.* **42**, 782–784.

Ulrich, A., Körner, H.J., Krötz, W., Ribitzki, G., Murnick, D.E., Matthias, E., Kienle, P. & Hoffmann, D.H.H. (1987). Heavy-ion excitation of rare-gas excimers. *J. Appl. Phys.* **62**, 357–361.

Ulrich, A., Wieser, J., Brunnhuber, A. & Krötz, W. (1994). Heavy ion beam pumped visible laser. *Appl. Phys. Lett.* **64**, 1902–1904.

Varentsov, D., Adonin, A., Fortov, V.E., Gryaznov, V.K., Hoffmann, D.H.H., Kulish, M., Lomonosov, I., Mintsev, V., Ni, P., Nikolaev, D., Shilkin, N., Shutov, A., Spiller, P., Tahir, N.A., Ternovoi, V. & Udrea, S. (2004). Report on December 2003 beamtime experiment at HHT: Near-critical HED states of lead generated by intense uranium beam. Scientific Report 2003. GSI: Darmstadt, Germany.

Wagner, T., Eberl, E., Frank, K., Hartmann, W., Hoffmann, D.H.H. & Tkotz, R. (1996). XUV amplification in a recombining z-pinch plasma. *Phys. Rev. Lett.* **76**, 3124–3127.

Young, R.J. De (1981). Kilowatt multiple-path ^{3}He-Ar nuclear-pumped laser. *Appl. Phys. Lett.* **38**, 297–298.

Ziegler, J.F., Biersack, J.P. & Littmark, U. (2003). Full description of the SRIM2003 code in the tutorial book. In *The Stopping and Range of Ions in Solids*. New York: Pergamon Press.

Zvorykin, V.D., Berthe, L., Boustie, M., Levchenko, A.O. & Ustinovskii, N.N. (2008). Planar shock waves in liquids produced by high-energy KrF laser: A technique for studying hydrodynamic instabilities. *Laser Part. Beams* **6**, 461–471.

Zvorykin, V.D., Didenko, N.V., Ionin, A.A., Kholin, I.V., Konyashchenko, A.V., Krokhin, O.N., Levchenko, A.O., Mavritskii, A.O., Mesyats, G.A., Molchanov, A.G., Rogulev, M.A., Seleznev, L.V., Sinitsyn, D.V., Tenyakov, S.Y., Ustinovskii, N.N. & Zayarnyi, D.A. (2007). GARPUN-MTW: A hybrid Ti:Sapphire/KrF laser facility for simultaneous amplification of subpicosecond/nanosecond pulses relevant to fast-ignition ICF concept. *Laser Part. Beams* **25**, 435–451.